

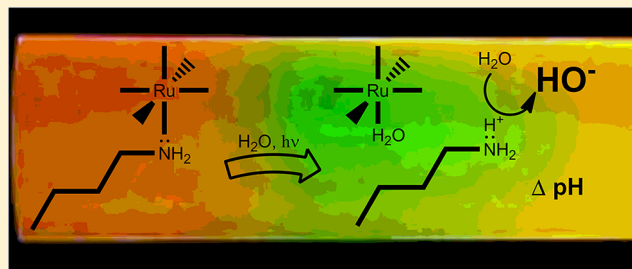
Fast Optical pH Manipulation and Imaging

Oscar Filevich, Guillermo Carrone, Victoria Andino Pavlovsky, and Roberto Etchenique*

Departamento de Química Inorgánica, Analítica y Química Física, INQUIMAE, Facultad de Ciencias Exactas y Naturales, Universidad de Buenos Aires, Ciudad Universitaria Pabellón 2, AR1428EHA Buenos Aires, Argentina

Supporting Information

ABSTRACT: We describe a complete system for optical pH manipulation and imaging. The system consists of a photoactive Ruthenium complex capable of inducing a change of more than 5 pH units at the nanosecond time scale. A compatible imaging system acquires microscopic pH images at 1200 fps using a nonexpensive commercial digital camera and an LED illumination system. We use the system as a superb tool to investigate flow in Flow Injection Analysis (FIA) models.



Imaging tools are being widely used in many fields. Several imaging techniques use low-throughput sensors to make an image through a scanning procedure. However, since the advent and popularization of digital cameras, the use of imaging techniques to quantify many parameters that vary in space and time has been much easier. In particular, fluorescent probes have proven to be very useful at measuring cytosolic $[Ca^{2+}]$ in biological systems,^{1,2} as a tool for microfluidic testing,³ in corrosion monitoring,⁴ and so forth. Fluorescent ratiometric tools for direct pH imaging have been developed and used in several applications.⁵ Digital images provide a high-throughput way to obtain raw data, which can be easily related to chemical and biochemical parameters with high spatial resolution.

However, to achieve good spatial and temporal resolution at the same time, enough light is needed to record an image in the millisecond range. In fluorescence mode, a high intensity excitation light source and very efficient microscope objectives together with expensive high speed, low noise CCD sensors are required.

Absorption spectrometry is often regarded as the poor sister of fluorescence based techniques. Its major drawback is an inherent lack of sensitivity due to the maximum molar absorptivity that an indicator usually shows, around $10^5 M^{-1} \text{cm}^{-1}$. Nevertheless, for a specimen of about $100 \mu\text{m}$ thick, and a concentration of 0.5 mM of such an indicator, an optimal absorbance of around 0.5 is obtained, allowing a precise measurement of the desired magnitude.

In fluorescence microscopy, fluorescent molecules emit photons in any direction, and the fraction captured by the objective is strongly dependent on its numeric aperture. Expensive objectives are thus required to improve this. In transmission microscopy, on the other hand, the lamp optics shoots an arbitrarily large amount of photons through the sample toward the objective. Some photons are captured by the sample, creating contrast in the image, but the amount of photons entering the objective can always be large. Thus, transmission microscopy images are usually much brighter than

fluorescence images. The amount of light entering the objective is not a limiting factor and high speed digital videophotography becomes easier to acquire, achieving high spatial and temporal resolution at very low cost.

On the other hand, optical pH manipulation has been demonstrated⁶ and used for biological measurements. The need of UV light to achieve the pH jump is an important issue of this kind of phototrigger, that needs quartz optics and expensive light sources or lasers to develop their full capabilities. We have developed a series of Ruthenium-based caged compounds, capable of blue, and even green absorption.^{7–9} These tools have been proven robust and were used to photodeliver neurotransmitters,⁸ bioactive chemicals,⁹ and to release protease inhibitors,¹⁰ and anticancer drugs.^{11,12} They worked as an excellent tool to determine circuitry in neuronal systems, even with single-spine resolution.^{13–16} In addition, they were also proven capable to stop epileptic seizures¹⁷ in animal models. Other kind of Ru complexes, based in a different photochemistry were used to photorelease nitric oxide.¹⁸ Rhenium complexes were recently tested for phototriggering electron flow in mutants of a blue copper protein *Pseudomonas aeruginosa* azurin.¹⁹ Ruthenium complexes are capable also of photoactivating a fluorescent dye.²⁰

We present in this paper a new system for pH manipulation and imaging comprising two main parts: a Ruthenium-bipyridyl complex capable of causing a shift of up to 6 pH units in the tens of nanoseconds range, and a compatible imaging tool using an indicator in absorption mode, an LED illuminated bright field microscope, and a commercial digital camera to image up to 1200 fps in a reliable way.

Received: March 1, 2012

Accepted: June 6, 2012

Published: June 6, 2012



■ EXPERIMENTAL SECTION

All reagents were commercially available and used as received. $[\text{Ru}(\text{bpy})_2(\text{PPh}_3)\text{Cl}] \text{Cl}$ and $\text{Ru}(\text{bpy})_2\text{Cl}_2$ were synthesized according to the literature using water as solvent.^{9,21} UV–Vis spectra were taken with a HP8453 diode-array spectrometer. NMR spectra were obtained using a 500 MHz Bruker AM-500. IR spectral measurements (KBr pellets) were carried out using a Nicolet 150P FTIR spectrophotometer. The photouncaging quantum yield measurements were performed with a 405 nm Solid State laser module with a constant power of 6.93 mW inside a fluorescence glass cuvette. The light was collimated and sent through an optical path of 1 cm into the cuvette, with stirring. Total irradiation energy was measured using a Coherent Fieldmaster FM light meter with a visible light photodiode model SR45. A similar laser module was focused on the capillary to generate the pulsed pH increase. The pulses were obtained by means of a function generator and a TIP122 transistor to drive the laser module.

Images of FIA capillaries were acquired using an inverted Nikon TS-100 microscope with bright field illumination. The illumination system of the microscope was replaced with a two-LED set, irradiating green (535 ± 16 nm fwhm) and red (635 ± 11 nm fwhm) light and placed in the same focal point using a dichroic mirror. Images were taken using a compact digital camera (Casio Exilim EX-FC100) which made focus through a normal eyepiece and a custom adapter and set to ISO 100 sensitivity. Videos and image analysis were done using public access *ImageJ* software.²²

Synthesis. $[\text{Ru}(\text{bpy})_2(\text{PPh}_3)(\text{BuNH}_2)]\text{Cl}_2$. A total of 200 mg of $[\text{Ru}(\text{bpy})_2(\text{PPh}_3)\text{Cl}] \text{Cl}$ was dissolved in 20 mL of water and heated to 80 °C. The formation of the $[\text{Ru}(\text{bpy})_2(\text{PPh}_3)(\text{H}_2\text{O})]^{2+}$ complex was determined by its absorption band at 425 nm which moves to 450 nm at pH > 12. After formation of the aquo complex, a mixture of 20 equiv of butylamine (BuNH_2) and 5 equiv of *p*-toluenesulfonic acid previously dissolved in 5 mL of water was added. The solution was heated at 80 °C in a sealed tube and monitored by UV–Vis during about 4 h, until no further spectral changes were observed. All the following procedures were done in darkness. The solution was filtered to remove any insoluble particles and the EtOH and the excess of BuNH_2 were removed under vacuum. The aqueous solution was precipitated with saturated KPF_6 . Yield: 65%. NMR (Acetone- d_6): ^1H δ 0.46 (t, 3H), 0.76 (m, 2H), 0.90 (m, 1H), 1.01 (m, 1H), 1.32 (m, 1H), 1.64 (m, 1H), 2.90 (t, 1H), 3.25 (t, 1H), 7.01 (t, 1H), 7.09 (t, 7H), 7.14 (t, 1H), 7.20 (t, 6H), 7.32 (d, 1H), 7.36 (t, 3H), 7.47 (t, 1H), 7.73 (t, 1H), 7.84 (d, 1H), 7.88 (t, 1H), 7.91 (t, 1H), 7.96 (d, 1H), 8.00 (d, 1H), 8.09 (t, 1H), 8.40 (d, 1H), 8.50 (d, 1H), 8.58 (d, 1H), 9.03 (d, 1H). Anal. Calcd: C, 67.36; H, 5.65; N, 9.35. Found: C, 67.1; H, 5.4; N, 9.5. Exchange of PF_6^- for Cl^- counterion was performed before use by suspending the complex in a 1:1 acetone–water mixture and a Dowex anion exchange resin. Acetone was removed under vacuum and the obtained solution was used directly.

■ RESULTS AND DISCUSSION

The main actuator in the described system is the complex $cis[\text{Ru}(\text{bpy})_2(\text{PPh}_3)(\text{BuNH}_2)]^{2+}$ (bpy = 2,2' bipyridine, PPh_3 = triphenylphosphine, BuNH_2 = *n*-butylamine), depicted in Scheme 1. This compound comprises two bidentate bipyridines coordinated to an octahedral Ru(II). Besides these two ligands, a monodentate PPh_3 is coordinated through its phosphorus,

Scheme 1. Molecular Structure and States Diagram of the Complex $cis[\text{Ru}(\text{bpy})_2(\text{PPh}_3)(\text{BuNH}_2)]^{2+}$

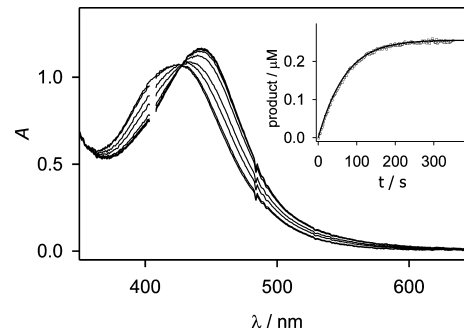
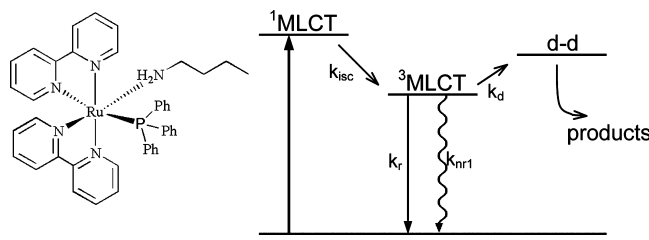


Figure 1. Photolysis of $[\text{Ru}(\text{bpy})_2(\text{PPh}_3)(\text{BuNH}_2)]^{2+}$ in aqueous solution, using a 405 nm laser module. The inset shows the number of moles of obtained products ($[\text{Ru}(\text{bpy})_2(\text{PPh}_3)(\text{H}_2\text{O})]^{2+}$ and butylamine), and the fit with a quantum yield $\Phi_{\text{pr}} = 0.165$ at pH = 7.

and the amine, in *cis* position, is coordinated through nitrogen. The photochemistry of this kind of complexes is widely known²³ and is depicted in Scheme 1. In brief, irradiation of the $^1\text{MLCT}$ band leads to an excited state in which one bipyridine receives electronic density from the metal center, formally Ru(III)-bpy^- . This singlet state decays to a triplet, from which a d–d metal centered nonbonding state can be populated. This d–d state promotes the heterolytic cleavage of one of the ligands in tens of nanoseconds.²⁴

As bipyridines are bidentate ligands, the probability of bipyridine cleavage is very low, usually undetectable. On the other hand, phosphines present a very strong bond to the Rutenium center,²⁵ and even poor bases as PPh_3 show no photodecomposition in the conditions used. As a result, a clean photoreaction yielding solely BuNH_2 and the aquo complex $[\text{Ru}(\text{bpy})_2(\text{PPh}_3)(\text{H}_2\text{O})]^{2+}$ is observed.

This photoreaction can be followed through UV–Vis spectrometry as can be seen in Figure 1.

The irradiation was performed using a 405 nm solid-state laser module. The presence of an isosbestic point shows that only two colored species are present: the original complex and the aquo complex. Given the power of the incident beam and the volume and concentration of the complex solution, it is possible to calculate the differential amount of product as:

$$\frac{dn_p}{dt} = I_{\text{beam}}(1 - 10^{-A_T}) \frac{A_R}{A_T} \cdot \Phi_{\text{pr}} \quad (1)$$

where n_p are the moles of uncaged product, I_{beam} is the intensity of the incident light in einsteins/s, A_T and A_R are the solution's total absorbance and the reactant's absorbance, respectively, and Φ_{pr} is the photoreaction quantum yield. The integration of eq 1 is done by a finite differences approach and the photorelease quantum yield is obtained, yielding $\Phi_{\text{pr}} = 0.165$, close to that of similar complexes.⁹ Curves with the fitted

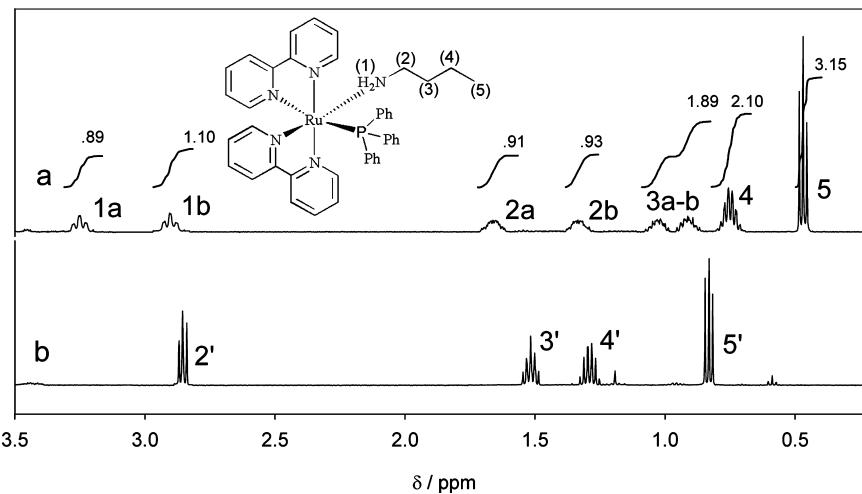


Figure 2. Photolysis of $[\text{Ru}(\text{bpy})_2(\text{PPh}_3)(\text{BuNH}_2)]^{2+}$ inside an NMR tube. (a) Aliphatic signals before irradiation correspond to coordinated BuNH_2 . Note the amine proton signals 1a and 1b. (b) after 3 min under a 450 nm LED, only the signals of free BuNH_2 (2',3',4', and 5') are visible.

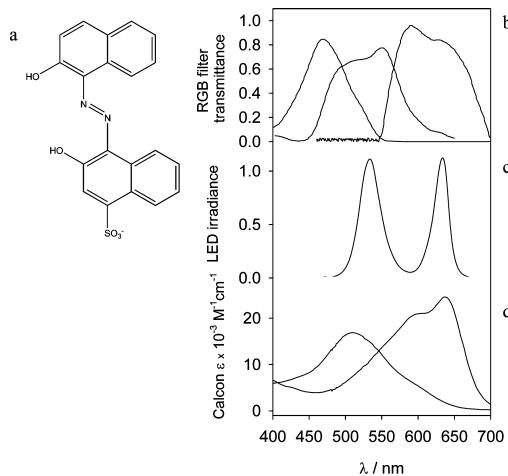


Figure 3. (a) structure of Calcon; (b) RGB filter transmittances on the camera; (c) emission of the illumination LEDs; (d) Calcon molar absorptivities at $\text{pH} = 4$ (left, absorbs mostly green light) and $\text{pH} = 10$ (right, absorbs mostly red light).

amount of photoreleased product versus irradiation time according to eq 1 are plotted in the inset, along with the corresponding experimental data.

The photoreaction was also followed by ^1H NMR spectroscopy and the results are shown in Figure 2. The characteristic

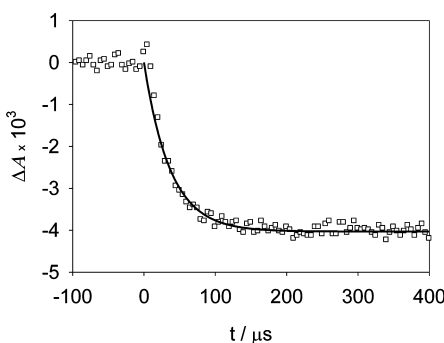


Figure 4. Absorbance transient for a solution containing 1.2 mM Calcon and 3 mM Ru complex at $\text{pH} = 4$ after irradiation with a Nd:YAG Q-Switched laser (532 nm, 7 ns, 0.5 J).

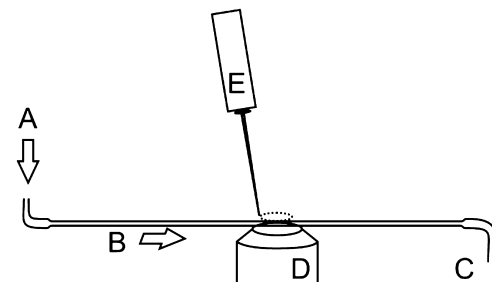


Figure 5. FIA capillary imaging at high speed. The inlet and outlet tubing (A, C) guide the flow through a FIA capillary (B) which is then discarded (C) after passing through the objective field (D). The complex $[\text{Ru}(\text{bpy})_2(\text{PPh}_3)(\text{BuNH}_2)]\text{Cl}_2$ is photolyzed by a 405 nm violet laser (E) increasing the pH and changing absorbance of Calcon, which is monitored at two wavelengths at high speed through a $10\times$ objective.

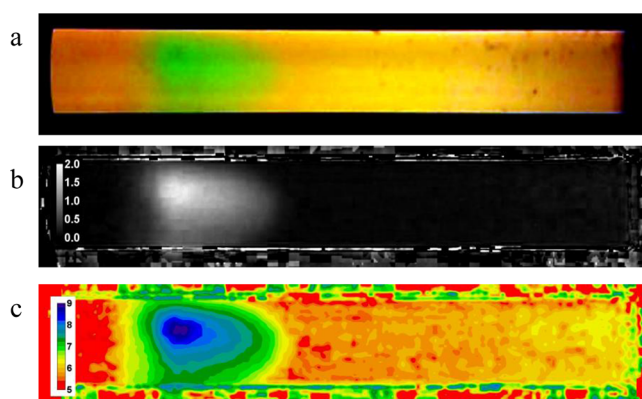


Figure 6. (a) Raw color image of a FIA capillary through which flows a solution containing 2 mM $[\text{Ru}(\text{bpy})_2(\text{PPh}_3)(\text{BuNH}_2)]\text{Cl}_2$ and 0.5 mM Calcon at $\text{pH} = 4$. The picture was taken 200 ms after a 20 ms laser pulse was directed to the capillary. (b) Monochrome image of deprotonated Calcon concentration (scale in mM) obtained from absorbance analysis of previous image. (c) False color image of pH calculated as $\text{pH} = \text{p}K_a + \log[x_B/(1 - x_B)]$.

signals of the 16 protons in bipyridines and the three broad peaks of PPh_3 are apparent in the aromatic region (see Supporting Information). The signals in the aliphatic region in

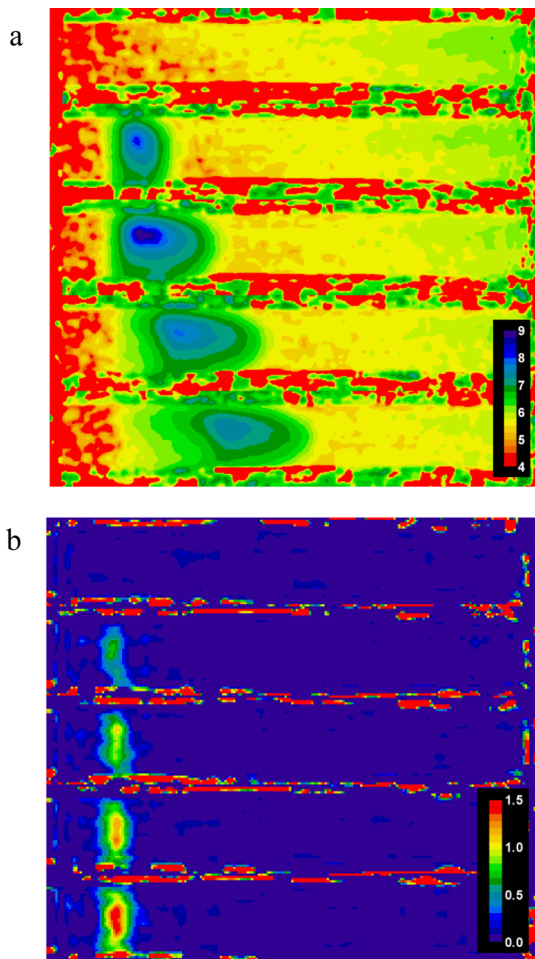


Figure 7. (a) False color pH images taken every 47.6 ms, from a video recorded at 210 fps. (b) False color base concentration taken every 1 ms from the beginning of the laser pulse. Scale in mM.

Figure 2a correspond to the coordinated butylamine. In particular, the triplets at 2.90 and 3.25 ppm are due to the coordinated $-\text{NH}_2$. These signals are stable in D_2O , showing that no isotopic exchange is possible in the coordinated amine, as expected for an electron pair involved in the coordination bond.

After irradiation inside the NMR tube with a 450 nm LED during 3 min, the original signals become negligible and the signals of the aquo complex in the aromatic region and that of free BuNH_2 in the aliphatic region appear without side reactions, which is the typical behavior of this family of complexes.^{9,24}

Butylamine is a rather strong base. Its conjugate cation has a $K_{\text{a}} = 10.77$. Coordinated butylamine, on the other hand, is not a base, given that the electron pair in the nitrogen is involved in the coordination bond. Thus, at millimolar concentrations, the photoreaction could be used to raise the pH value up to 11. The actual upper limit will be somewhat lower, due to the fact that the aquo complex $[\text{Ru}(\text{bpy})_2(\text{PPh}_3)(\text{H}_2\text{O})]^{2+}$ is a very weak acid that deprotonates to $[\text{Ru}(\text{bpy})_2(\text{PPh}_3)(\text{OH})]^+$ with $pK_{\text{a}} \approx 10$, buffering the system above this pH value. Flash photolysis measurements were done using a Nd:YAG Q-switched 532 nm laser and recording the changes in absorbance due to loss of the ligand. After irradiation, butylamine is released to the medium with $t_{1/2} = 22$ ns, showing a similar value to other complexes of the family.^{7,24} This defines the

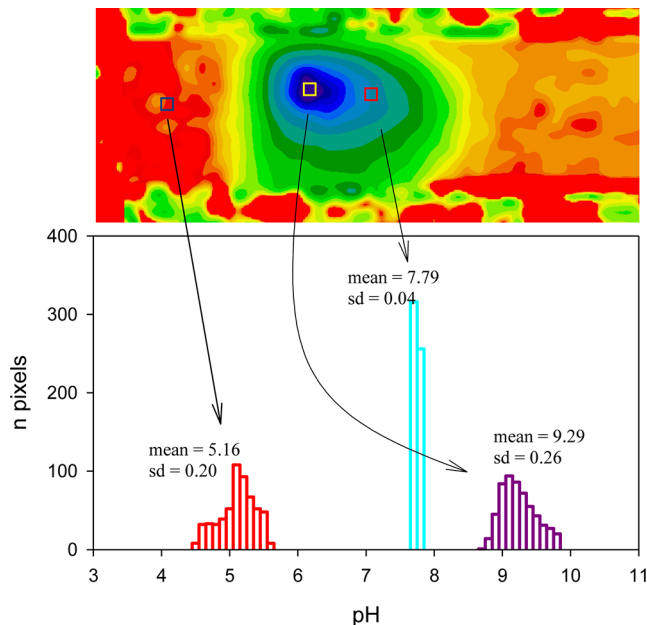
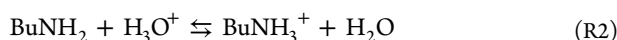
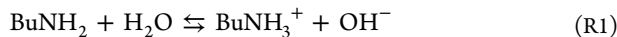


Figure 8. Histograms showing dispersion of obtained pH values at pH = 5.16, pH = 7.79, and pH = 9.29. The noise increases when pH is far from pK_{a} due to the low concentration of one of the two indicator species. Histograms are obtained from a 20×20 pixels square in single frames taken at 210 fps.

maximum theoretical rate of the pH jump. However, the amine protonation equilibrium and diffusion have also to be taken into account. Water and butylamine need to diffuse and encounter for the proton exchange reaction to take place through one of the following reactions:



To estimate the maximum rate of the forward reaction due to diffusion control, some calculations can be done. For two molecules of diffusion coefficients D_A and D_B and reaction distance R , the diffusion rate constant is

$$k_d(\text{M}^{-1} \text{s}^{-1}) = 4 \times 10^3 \pi R(D_A + D_B)N_A$$

where N_A is Avogadro's constant.

Water self-diffusion coefficient is $D_W = 2.1 \times 10^{-9} \text{ m}^2 \text{ s}^{-1}$ and butylamine diffusion coefficient in water is $D_B = 8.7 \times 10^{-10} \text{ m}^2 \text{ s}^{-1}$. We can use the Stokes-Einstein relation to estimate their effective radii $a = k_B T / 6\pi\eta D$, where k_B is the Boltzmann constant and T the temperature, to obtain $a_W = 0.12 \text{ nm}$ and $a_B = 0.28 \text{ nm}$. Considering the reaction distance $R \cong R_W + R_B = 0.40 \text{ nm}$, we can estimate $k_d \cong 9 \times 10^9 \text{ M}^{-1} \text{ s}^{-1}$, which is a typical value for diffusion controlled rate constants. With water present at 55.5 M, the pseudo first order is $k_d' \cong 5 \times 10^{11} \text{ s}^{-1}$, corresponding to a $t_{1/2} = 1.4 \text{ ps}$, much faster than the photorelease process. This is a consequence of the very high concentration of water molecules in the vicinity of any amine molecule. On the other hand, for the reaction of the amine with H_3O^+ , similar considerations give a value of $t_{1/2} = 75 \text{ ns}$ at pH = 3. The kinetics of protonation for some aliphatic amines has been measured. For methylamine, analogue of butylamine, the first-order rate constant for the forward reaction of eq R1 is $k_1 = 1.2 \times 10^7 \text{ s}^{-1}$, corresponding to a $t_{1/2}$ of 58 ns, and the

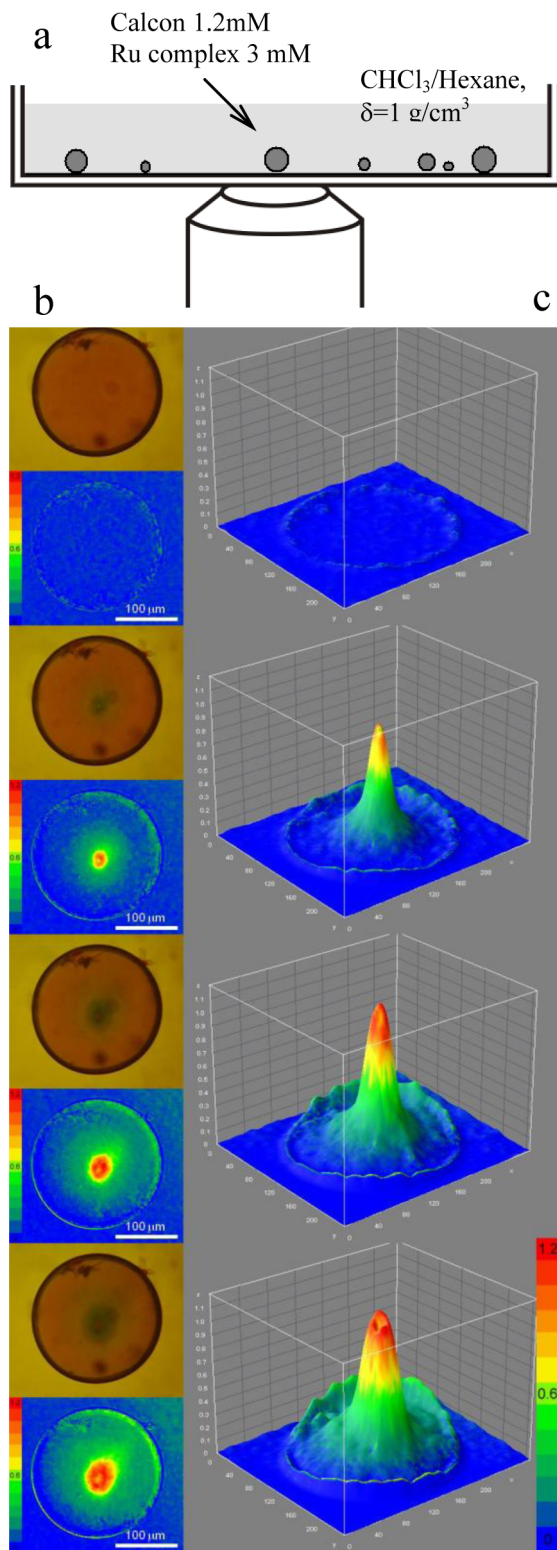


Figure 9. (a) Scheme of the experimental configuration used for imaging diffusion in droplets. (b) A sequence of 4 snapshots of a full video. Top: Unprocessed microscope image. Bottom: false color quantification of the basic form of Calcon in each pixel. Color scale in mM. (c) Surface plots corresponding to the pictures on the left.

second-order forward rate constant for eq R2 is $k_2 = 3.7 \times 10^{10} \text{ M}^{-1} \text{ s}^{-1}$, which at pH = 3 corresponds to a $t_{1/2}$ of 18 ns.

In conclusion, all the rate constants for the steps between irradiation and the actual pH jump lie around the tens of

nanoseconds or less, with probably the reaction between amine and H₂O the rate-determining step. However, even if the pH jump occurs very rapidly, the measurement of such changes will be limited by the indicator reaction rates (see below). The described properties make this system an ideal pH photoactuator capable of increasing the pH from 3–4 to 10 in a fast, reliable, and easily controlled way. Other similar complexes bearing amines as ligands can be used for the same purposes. The caged amino acids [Ru(bpy)₂(PPh₃)(GABA)]⁺ and [Ru(bpy)₂(PMe₃)₂(Glut)] have the advantage of their higher water solubility,^{9,24} although the carboxyl group prevents the jump at initial pH lower than 5 due to its buffer power.

Calcon is a sodium salt of 1-(2-hydroxy-1-naphthylazo)-2-naphthol-4-sulfonic acid which is used in complexometric titrations of calcium.²⁶ Its structure is shown in Figure 3a. Its phenolic group allows its use as a pH indicator with $pK_a = 7.40$. In the mononegative form (due to the presence of the $-\text{SO}_3^-$ group), Calcon presents a maximum in absorbance at 515 nm, while its deprotonated anion shows a strong absorption around 640 nm (Figure 3d). Contrary to most pH indicators, the maximum molar absorptivities of both species is rather similar. This property, and the fact that the position of the bands overlap in a good extent with the maxima of digital camera color filters (Figure 3b), makes Calcon an ideal indicator for digital photometric measurement of pH around 7.

Calcon presents maxima of $24500 \text{ M}^{-1} \text{ cm}^{-1}$ for the basic form at 635 nm and of $14\,700 \text{ M}^{-1} \text{ cm}^{-1}$ for the acid form at 535 nm. The high extinction coefficients of Calcon in both its acid and basic forms guarantee that the small differences of Ru complex absorption after photoreaction (see Figure 1) can be considered negligible. The complex molar absorptivities at 535 nm change from $344 \text{ M}^{-1} \text{ cm}^{-1}$, while at 635 nm, its absorption is almost zero.

To obtain a reliable measure of absorbance using a digital camera, the color channels should be fed with monochromatic light. Although laser illumination would be optimal to achieve this goal, it introduces speckle into the image. LED illumination, on the contrary, presents no such spectral purity but results in a more homogeneous light field. White LEDs offering a broad light spectrum have been used for quantitative analysis using RGB cameras in normal (slow) mode.²⁷ Some works use monochromatic LED excitation,^{28,29} providing the RGB measurement from the emission of the sample. In our case, we extend these techniques to very fast measurements using camera with a fast CMOS sensor and a combined dual wavelength high power LED source to diminish error in absorbance determination. We chose LEDs as light sources, at 535 ± 16 and $635 \pm 11 \text{ nm fwhm}$ respectively, as depicted in Figure 3c. Both emitters are placed colinear using a dichroic mirror. Under this illumination, the acid form of Calcon appears orange and the basic form appears green. The blue channel of the digital camera was not used for measurement purposes.

This devised pH actuation-measurement chemical system is a powerful tool that can be used in many ways. We have tested the system to image the flow in a FIA capillary under the microscope, at a speed of 30–1000 frames/s (fps). Microscopic flow imaging in FIA or microfluidic devices is done with caged-fluorophores present weak or no fluorescence until an uncaging light of the adequate wavelength activates them. The principal drawback of this kind of dyes is that fluorescence is difficult to measure in very fast video-microscopy, because of the limited amount of light that can be

collected in short times. On the other hand, almost any camera can be used in bright field microscopy, including cheap slow-motion digital cameras capable of imaging up to 1200 fps video during several minutes. Our combination of pH actuation and absorption measurement is ideal to achieve high resolution pH videos at very high frame rates.

The time resolution of the imaging system will be limited by the reaction rate of the indicator. For a typical indicator such as phenolphthalein, the rate of the forward reaction in the equilibrium InH^- (colorless) + $\text{OH}^- \rightleftharpoons \text{In}^{2-}$ + H_2O (pink) has been determined to be $k_1 = 2 \times 10^9 \text{ M}^{-1} \text{ s}^{-1}$, which implies that at the usual working concentrations, the color change of the indicator is much slower than the pH change induced by the light pulse.³¹

In the case of Calcon, there are no kinetic studies regarding its use as pH indicator. Therefore, we conducted flash photolysis experiments in order to determine the rate of the absorbance change in our experimental conditions. A sample containing 1.2 mM Calcon and 3 mM Ru complex at pH = 4 was placed in a 0.1 mm optical path flow cell, and its absorbance was measured using a 655 nm laser diode as light source. Laser pulses of 0.5 J and 7 ns were used to irradiate the sample. The result is shown in Figure 4.

The monoexponential decay can be fitted given the $t_{1/2} = 26.1 \mu\text{s}$. The rate of the photolysis is linearly dependent on the concentration of the indicator. By changing the concentration of Calcon, keeping pseudo-first-order conditions, the second-order kinetic constant for the reaction: $\text{CalconH}^- + \text{OH}^- \rightarrow \text{Calcon}^{2-} + \text{H}_2\text{O}$ can be calculated to be $k_1 = 2.22 \times 10^7 \pm 0.09 \text{ M}^{-1} \text{ s}^{-1}$. Other indicators, such as bromothymol blue, show faster responses, closer to that of phenolphthalein, but their absorption wavelengths do not match the wavelengths of the CCD camera filters as well as those of Calcon. With our photographic system in the milliseconds range, a response in the tens of microseconds is perfectly useful, even though for faster cameras other indicators should be used.

The imaging scheme is depicted in Figure 5. The FIA-size capillary is imaged through a 10 \times objective in an inverted microscope using 535 and 635 nm LEDs as light sources. A continuous flow of a solution containing 2 mM [Ru(bpy)₂(PPh₃)(BuNH₂)]Cl₂ and 0.5 mM Calcon, to which HCl was added until pH = 4.00, was driven by gravity. At a fixed point in the capillary, a focused 405 nm laser was pulsed at a constant rate.

The digital camera was set to its minimum sensitivity (ISO 100) to minimize noise. The videos can be taken at 30, 210, or 1000 fps, adjusting the light intensity to allow a precise measurement at such speeds. The image frame at 30 fps is over 6 Megapixel resolution, and around 100 kpixel at the highest speed.

Figure 6a shows a typical raw RGB image taken at 210 fps. Image decomposition in R, G, and B colors (B is discarded) allows precise determination of the absorbance at 535 and 635 nm. Prior to this determination, the linear range of the response must be determined. This can be done using Calcon solutions of known absorbance at both wavelengths at buffered pH. The R and G pixels result to be rather linear between 35 and 210 counts, which cover the 68% of the entire light intensity range, and are suitable for the measurements with the required precision. The light level of both LED sources was adjusted to fit this linear range. During the measurement of pH *in-line*, distilled water or a solution containing only the Ru complex, which does not present absorption above 480 nm, can be used

as reference for absorbance measurement. However, it is easier to use a nonirradiated portion of the video to get the baseline. Both procedures gave the same results, and the second was chosen for simplicity. Concentrations of the basic and acid species can be obtained simply by applying Beer's law, and the local pH is calculated from these values. The results are shown in Figure 6, panels b and c, respectively.

Concentration and pH images can be taken at millisecond rate. Figure 7a shows selected frames of a video at 210 fps. Frames shown were taken every 47.6 ms. A much faster sequence at the beginning of the laser pulse, taken every 1 ms and depicting the deprotonated Calcon concentration, is shown in Figure 7b. (The corresponding videos are available as Supporting Information.)

The pH measurement can be very precise near the pK_a of Calcon, but the reliability obviously decreases when any one of the species becomes scarce. Figure 8 shows typical histograms of 400 pH pixels at different positions in the picture.

Even though some of the spread is due to real changes of pH in the measured area, particularly where pH gradient is higher, most of the dispersion is due to measurement error. Around pH = 7.8, standard deviation is $\sigma_{\text{pH}} = 0.04$, while at pH near 5 or 9, it increases to $\sigma_{\text{pH}} = 0.20$ and $\sigma_{\text{pH}} = 0.26$, respectively, although in some regions can be somewhat higher. Concentration measurements, on the other hand, present a relative dispersion between 6% and 12% within a 400 pixel square, before applying any spatial filtering. Contrary to the simple measurement of precision, accuracy is difficult to estimate, and has to be done at slow speed, by changing the pH of the carrier without altering the concentration, and measuring the solution pH independently. Using a glass electrode, differences of ± 0.06 pH units were obtained for pictures taken at 420 fps, using 20 \times 20 pixel averages between pH 5.5 and 8.5 at 25 °C. Differences are higher when pH is farther from the indicator pK_a.

The presented method not only allows for the fast measurement of pH, but it is also good for obtaining qualitative images of flow inside the capillary or any other translucent microdevices. These images are even better than those obtained using caged fluorescent probes.²⁰ This is due to the possibility of decreasing the ISO gain of the CCD sensor, reducing noise and increasing the SNR, simply by increasing the illumination power directed through the sample. The pH measurement method is ratiometric; moreover, it is robust against a small amount of photobleaching, which can appear when very high laser power density is used to change the pH. Alternatively, increasing illumination also allows for an increase in the frame rate without sacrificing SNR. In our equipment, the maximum possible frame rate was determined by the camera's features and required only moderate illumination, only a fraction of the excitation light required for the typical fluorescence microscope.

We have devised this method mainly to help visualization of flow and pH variations in microfluidics circuits and FIA systems, which are in continuous development nowadays. The new techniques to pump liquids in microdevices in the order of tens and hundreds of micrometers will surely allow new goals in the analysis of microsamples with high throughput.³² However, many other kind of measurements can also be done. As an example, Figure 9a depicts a method to measure the change of pH due to the diffusion of the photolyzed base into a stationary spherical drop with a size of a big cell (200 μm diameter). A 45/55% (v/v) mixture of chloroform and *n*-hexane, which density is slightly lower than that of water, is prepared. A drop of a

aqueous solution containing 1.2 mM Calcon and 3 mM Ru at pH 4 is placed in the organic mixture, and is divided into very small droplets with vigorous agitation. This suspension is then poured into a glass Petri dish and sealed to prevent evaporation. The droplets, with a size ranging from 10 to 500 μm , can be individually addressed with an inverted microscope.

A pulsed 405 nm laser spot (diameter = 800 nm) is directed through the microscope optics using a dichroic mirror and a slow-motion video is taken at 210 fps.

Sequence in Figure 9b shows the raw image obtained (true color) and the concentration of the indicator base in millimolar (mM) (false color) at four different times of irradiation. The corresponding frames in Figure 9c show the surface plot of the indicator base concentration in the z axis.

The black border in the raw image and the corresponding colors in the “crown” that appear at the edge of the droplet are not pH related. Note that after continuous irradiation (fourth frame), some photobleaching appears at the laser focal point. A video in slow motion is available as Supporting Information.

In conclusion, we have developed a system composed of a caged amine, which is used as a molecular actuator to increase more than 5 pH units in the submicrosecond range, and a fast and reliable measurement method based in the indicator Calcon. As a proof of principle, diffusion in a 200 μm drop and pH increase into a FIA system can be followed *in situ* using a nonexpensive digital camera capable of recording videos with up to 1000 fps. This last experiment allows the researcher to visualize in a very accurate way the parabolic profile of velocities inside any microfluidic channel without any disturbing mixture device. In this way, information on the laminar and/or turbulent flow in FIA and lab-on-a-chip devices can easily be obtained in a straightforward way.

As the amount of transmitted light can be modified, even faster recording can be achieved by means of a higher speed CCD sensor. In absorbance mode, light can be directed with precision through the specimen in analysis to the objective. This is an important advantage over the use of caged-fluorescent dyes, which emit light in all directions and need high aperture optics to guarantee enough light intensity at the detector.

This new approach to optical manipulation/imaging is therefore an excellent tool to measure pH in a fast and reliable way with very low cost of use and implementation.

ASSOCIATED CONTENT

Supporting Information

NMR, IR, and UV–Vis spectra of the butylamine complex and videos corresponding to the data depicted in Figures 6, 7, and 9. This material is available free of charge via the Internet at <http://pubs.acs.org>.

AUTHOR INFORMATION

Corresponding Author

*E-mail: rober@qi.fcen.uba.ar.

Notes

The authors declare no competing financial interest.

ACKNOWLEDGMENTS

This research was supported by the National Agency for Science and Technology Promotion (ANPCyT 00321) and the University of Buenos Aires (UBACyT X075). R.E. is a staff

member of CONICET. Fruitful discussions with Mabel Tudino and her invaluable assistance are highly appreciated.

REFERENCES

- (1) Clark, H. A.; Kopelman, R.; Tjalkens, R.; Philbert, M. A. *Anal. Chem.* **1999**, *71*, 4837–4843.
- (2) Alonso, M. T.; Barrero, M. J.; Michelena, P.; Carnicero, E.; Cuchillo, I.; García, A. G.; García-Sancho, J.; Montero, M.; Alvarez, J. *J. Cell. Biol.* **1999**, *144*, 241–254.
- (3) Wolff, A.; Perch-Nielsen, I. R.; Larsen, U. D.; Friis, P.; Goranovic, G.; Poulsen, C. R.; Kutterer, J. P.; Telleman, P. *Lab Chip* **2003**, *3*, 22–27.
- (4) Augustyniak, A.; Tsavalas, J.; Ming, W. *ACS Appl. Mater. Interfaces* **2009**, *1* (11), 2618–2623.
- (5) Charier, S.; Ruel, O.; Baudin, J. B.; Alcor, D.; Allemand, J. F.; Meglio, A.; Jullien, L. *Angew. Chem., Int. Ed.* **2004**, *43*, 4785–4788.
- (6) Abbruzzetti, S. S.; Sottini, S. S.; Viappiani, C. C.; Corrie, J. E. T. *J. Am. Chem. Soc.* **2005**, *127* (27), 9865–9874.
- (7) Filevich, O.; Salierno, M.; Etchenique, R. *J. Inorg. Biochem.* **2010**, *104*, 1248–1251.
- (8) Zayat, L.; Calero, C.; Alborés, P.; Baraldo, L.; Etchenique, R. *J. Am. Chem. Soc.* **2003**, *125*, 882–883.
- (9) Zayat, L.; Noval, M. G.; Campi, J.; Calero, C. I.; Calvo, D. J.; Etchenique, R. *ChemBioChem* **2007**, *8*, 2035–2038.
- (10) Respondek, T.; Garner, R. N.; Herroon, M. K.; Podgorski, I.; Turro, C.; Kodanko, J. *J. Am. Chem. Soc.* **2011**, *133*, 17164–17167.
- (11) Garner, R. N.; Gallucci, J. C.; Dunbar, K. R.; Turro, C. *Inorg. Chem.* **2011**, *50*, 9213–9215.
- (12) Goldbach, R. E.; Rodriguez-Garcia, I.; van Lenthe, J. H.; Siegler, M. A.; Bonnet, S. *Chem.—Eur. J.* **2011**, *17*, 9924–9929.
- (13) Crandall, S. R.; Cox, C. L. *J. Neurosci.* **2012**, *32*, 2513–2522.
- (14) Poskanzer, K. E.; Yuste, R. *Proc. Natl. Acad. Sci. U.S.A.* **2011**, *108*, 18453–18458.
- (15) Yuste, R. *Neuron* **2011**, *71*, 772–781.
- (16) Woodruff, A. R.; McGarry, L. M.; Vogels, T. P.; Inan, M.; Anderson, S. A.; Yuste, R. *J. Neurosci.* **2011**, *31*, 17872–17886.
- (17) Yang, X.; Rode, D. L.; Peterka, D. S.; Yuste, R.; Rothman, S. M. *Ann. Neurol.* **2012**, *71*, 68–75.
- (18) Ortiz, M.; Torréns, M.; Mola, J. L.; Ortiz, P. J.; Fragoso, A.; Díaz, A.; Cao, R.; Prados, P.; de Mendoza, J.; Otero, A.; Antíñolo, A.; Lara, A. *Dalton Trans.* **2008**, 3559–3566.
- (19) Blanco-Rodríguez, A. M.; Di Bilio, A. J.; Shih, C.; Museth, A. K.; Clark, I. P.; Towrie, M.; Cannizzo, A.; Sudhamsu, J.; Crane, B. R.; Sýkora, J.; Winkler, J. R.; Gray, H. B.; Záliš, S.; Vlček, A. *Chem.—Eur. J.* **2011**, *17*, 5350–5361.
- (20) del Marmol, J.; Filevich, O.; Etchenique, R. *Anal. Chem.* **2010**, *82*, 6259–6264.
- (21) Viala, C.; Coudret, C. *Inorg. Chim. Acta* **2006**, *359*, 984–989.
- (22) Abramoff, M. D.; Magalhaes, P. J.; Ram, S. J. *Biophotonics Int.* **2004**, *7*, 36–42.
- (23) Campagna, S.; Puntoriero, F.; Nastasi, F.; Bergaminim, G.; Balzani, V. *Top. Curr. Chem.* **2007**, *280*, 117–214.
- (24) Salierno, M.; Merceca, E.; Peterka, D. S.; Yuste, R.; Etchenique, R. *J. Inorg. Biochem.* **2010**, *104*, 418–422.
- (25) Sullivan, B. P.; Salmon, D. J.; Meyer, T. J. *Inorg. Chem.* **1978**, *12*, 3334–3341.
- (26) Hildebrand, G. P.; Reilley, C. N. *Anal. Chem.* **1957**, *29* (2), 258–264.
- (27) Tang, Z.; Yang, J.; Yu, J.; Cui, B. *Sensors* **2010**, *10*, 6463–6476.
- (28) Steiner, M. S.; Meier, R. J.; Duerkop, A.; Wolfbeis, O. S. *Anal. Chem.* **2010**, *82*, 8402–8405.
- (29) Wang, X. D.; Meier, R. J.; Link, M.; Wolfbeis, O. S. *Angew. Chem., Int. Ed.* **2010**, *49*, 4907–4909.
- (30) Ross, D.; Johnson, T. J.; Locascio, L. E. *Anal. Chem.* **2001**, *73*, 2509–2515.
- (31) Massey, M. W.; Schelly, Z. A. *J. Phys. Chem.* **1978**, *78* (24), 2450–2454.
- (32) Leslie, D. C.; Easley, C. J.; Seker, E.; Karlinsey, J. M.; Utz, M.; Begley, M. R.; Landers, J. P. *Nat. Phys.* **2009**, *5*, 231–235.